The sol to gel transition in irreversible particulate systems

C. M. Sorensen* and A. Chakrabarti

Received 9th April 2010, Accepted 27th September 2010
DOI: 10.1039/c0sm00228c

A review of the process by which irreversible aggregation of solid particles creates fractal aggregates which eventually fill the entire system volume to form a gel, the sol to gel transition, is presented. Both simulation and experiment present a coherent description of the kinetics and resulting morphologies of this process. Enhanced kinetics occurs when the system is cluster dense. Surprisingly, the enhanced kinetics is governed by the mean-field Smoluchowski equation deep into the aggregation process, displays universality with cluster volume fraction (or, equivalently the ratio of cluster separation to size, or time normalized by the gel time), and is described by one parameter, the aggregation kernel homogeneity. Aggregates show canonical cluster–cluster morphology until the point where the cluster volume fraction is unity; then hybrid superaggregates with fractal dimensions of *ca.* 1.8 over small length scales and 2.6 over large length scales form.

1 Introduction

Gels are semirigid dispersions of a solid in a liquid or gas. Both phases have large scale connectivity spanning across the macroscopic boundaries of the system. The solid phase is typically the minority phase often on the order of 1% of the total volume. Gels are ubiquitous in nature and technology[1] and are found in far ranging contexts such as self-associating polymer networks, biological systems, the synthesis of catalytic supports and even soot aerosols.

The dominant description of gelation has been the percolation theory[2] which has seen considerable success and use. Percolation theory, however, does not attempt to describe the kinetics of the gelation process, *i.e.*, how the sol evolves to the gel. Moreover, as we will see, percolation theory misses an important aspect of the morphology of the clusters that form the gel network.

Here we present a description of how gels form from the precursor sol *via* the processes of aggregation and gelation. The distinction between these two processes has a nebulous boundary but one can assert that "aggregation" is the process of forming clusters (synonymous with aggregates) from smaller entities, and "gelation" is the process of forming a volume spanning gel, again from smaller entities. The limiting feature to aggregation is that the entities are relatively very far apart, whereas with gelation they are quite close together. A primary motive of this review is to connect these two processes by spanning the gap between these inherent length scales into a unified description of how gels form. Furthermore, here we consider aggregation such that when two aggregates do in fact stick together they remain stuck together. This is a very common situation and can serve as a frame of reference for other situations where the binding is not permanent. However, the fundamental physical concepts to be discussed here underlie all these gels. These more general cases have seen useful reviews previously.[3,4]

Department of Physics, Kansas State University, Manhattan, Kansas, 66506-2601, USA. E-mail: sor@phys.ksu.edu; amitc@phys.ksu.edu; Tel: +785-532-1626 (C. M. Sorensen); +785-532-1625 (A. Chakrabarti)

2 Why systems gel

Gels form from a dispersion because, when destabilized to allow aggregation, the non-coalescing solid phase forms aggregates (or clusters) with a scaling dimensionality less than the spatial dimensionality. Thus the total aggregate volume consumes space as the aggregates grow until there is no free, non-aggregate space remaining.

The non-dense nature of the aggregates is described by their mass–radius scaling law

$$N = k_0(R_g/a)^{D_f} \quad (1)$$

Here N is the aggregate's "mass", the number of monomers of radius a in the aggregate; R_g is the aggregate's radius of gyration, a root-mean-square radius, which is a measure of its linear size; k_0 is the prefactor of order unity; and D_f is the aggregate's fractal dimension with a value less than the spatial dimension, d. It follows from eqn (1) that

$$R_g \sim N^{(1/D_f)} \quad (2)$$

The mean nearest neighbor separation R_{nn} is controlled by the spatial dimension. It is related to the total number of clusters N_c in the system of volume V by

$$R_{nn} \sim (N_c/V)^{-(1/d)}. \quad (3)$$

In a mass conserving system the total number of monomers in the system N_m is constant. Under the assumption of the clusters (or synonymously aggregates) having the same size, one has $N_m = N_c N$. Then from eqn (3) it follows

$$R_{nn} \sim N^{1/d}. \quad (4)$$

Typically, in a given sol (colloid or aerosol), the aggregates are far apart relative to their average nearest neighbor separations, *i.e.* $R_{nn} \gg R_g$. However, as aggregation proceeds, as described by the increasing cluster mass N, eqn (2) and (4) show that since d $> D_f$, R_g will increase faster than R_{nn} and will eventually catch

up with it. When it does, *i.e.*, when $R_{nn} \sim R_g$, the system gels (almost, see below) as already mentioned by Kolb *et al.*[5] and Vicsek.[6] Thus, simply said: systems gel because $D_f < d$.† This is displayed in Fig. 1.

Fig. 1 shows a sketch of the behavior of R_g and R_{nn} as a function of the mean number of monomers per aggregate $<N>$ which grows with time as the aggregation proceeds. When $R_{nn} \gg R_g$, the aggregates are relatively very far apart, a situation we call *cluster dilute*. As the aggregation proceeds, Fig. 1 shows that both R_{nn} and R_g grow, but the relative cluster separation R_{nn}/R_g decreases with time. Below we will show that when this ratio decreases to about 10, changes occur in the aggregation kinetics due to cluster crowding. Thus the system enters what we have called the *cluster dense* regime. These two regimes are identified in Fig. 1. Well into the cluster dense regime the aggregates grow to the point that they fill the entire system volume. Then neighboring clusters will touch and the cluster volume fraction equals one. We define this point as the *ideal gel point*.[7] Its approximate condition is when $R_{nn} \sim R_g$ as indicated in Fig. 1. Beyond the ideal gel point, the fractal clusters interdigitate. Eventually a system spanning cluster forms marking the *physical gel point*. Continued aggregation after the gel point involves incorporation of the remaining material into the spanning gel until every monomer is part of the same network, a point called the *final gel state*.[8,9]

The cluster occupied volume includes everything, connected monomers and the space between them, within the perimeter of the cluster. A cluster perimeter is ill defined but one can argue that in analogy to a sphere the perimeter radius can be described by $R_p = [(D_f + 2)/D_f]^{(1/2)}R_g$.[10] Then assuming all the clusters are the same size and are spherical, the total cluster volume fraction is

$$f_{v,c} = (4\pi/3)(N_c/V)[(D_f + 2)/D_f]^{3/2}\ R_g^{\ 3} \tag{5}$$

Then the ideal gel point is defined as when $f_{v,c} = 1$.[7] For fractal aggregates with $D_f = 1.8$, this is equivalent to $R_{nn} = 2.3R_g$. The free volume can pass through zero and become negative, thus marking a regime of cluster interdigitation.

The size of the clusters at the ideal gel point will be designated as $R_{g,G}$, the radius of gyration at the ideal gel point.[11] Setting $f_{v,c} = 1$ in eqn (5), using eqn (1) and conserving mass through $N_m = N_c N$, one finds

$$R_{g,G} = a[f_{v,m}^{-1}k_0(D_f/(D_f + 2))^{3/2}]^{1/(3\ -\ D_f)} \tag{6}$$

where the monomer volume fraction is given by $f_{v,m} = N_m(4\pi/3)a^3/V$.

† Consider, in contrast, a system of coalescing liquid droplets; rain drops in a cloud for example. Imagine the time when the mean droplet diameter is 1 micron and the mean droplet nearest neighbor separation is 10 microns; a ten-to-one ratio. Now let time pass and the system evolve *via* aggregation to larger droplets, say one millimetre mean diameter. Question: now what is the mean nearest neighbor separation? Answer: 10 millimetres. Because liquid droplets coalesce when they aggregate, their mass–size scaling exponent, *i.e.*, their fractal dimension is $D_f = 3$. This is equal to the spatial dimension, $D_f = d = 3$. Thus the separation to size ratio remains the same at ten-to-one because the droplet dimensionality is the same as the spatial dimensionality.

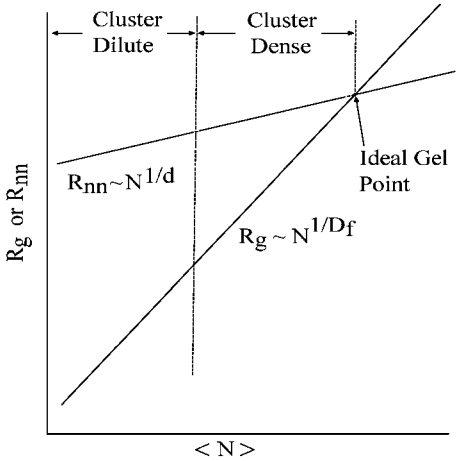

Fig. 1 Sketch of the evolution of the two primary length scales in an aggregating sol *versus* the mean number of monomers per aggregate $<N>$. The length scales are the aggregate radius of gyration, R_g, and the aggregate mean nearest neighbor separation, R_{nn}. The functionalities of these length scales are governed by the aggregate fractal dimension, D_f, and the spatial dimension, $d > D_f$. Cluster dilute ($R_{nn} \gg R_g$) and cluster dense ($R_{nn} \geq R_g$) regimes are indicated. The ideal gel point is when these two length scales are approximately equal.

3 The kinetics of the sol–gel transition

3.1 The Smoluchowski equation

When cluster dilute, aggregation kinetics is governed by the Smoluchowski equation (SE), expressing the change in cluster concentration $n(k)$ for k monomers per cluster as[12,13]

$$\frac{dn(k)}{dt} = \frac{1}{2}\sum_{i=1}^{i=k-1} K(i,k-i)n(i)n(k-i) - n(k)\sum_{i=1}^{\infty} K(i,k)n(i) \tag{7}$$

where $K(i,j)$ is the aggregation kernel. The SE is based on the mean-field assumption that there are no spatial correlations between clusters; hence the probability of two clusters meeting is simply proportional to the product of their number densities. For many physical situations the aggregation kernel is a homogeneous function,

$$K(ai,aj) = a^{\lambda}K(i,j) \tag{8}$$

where λ is the degree of homogeneity. Then the SE yields self-preserving scaling solutions[14,15]

$$n(k) = M_1 s_p^{-2}\ \varphi(x) \tag{9}$$

where M_1 is the first moment of the size distribution and $s_p = M_p/M_{p-1}$, where M_i is an ith moment, is a mean cluster size. The scaling function $\varphi(x)$ in eqn (9) is given by

$$\varphi(x) = Ax^{-\lambda}\ e^{-\alpha x} \tag{10}$$

where $x = k/s_p$ is the scaled size and A and α are normalization constants near unity. Eqn (10) is valid for $x > 1$. Substituting (9) into the SE, one finds that the moments of the size distribution obey

$$M_i(t) = M_i(0)\,(1 + t/t_c)^{(i-1)z} \quad (11)$$

where t_c is a characteristic time and

$$z = 1/(1 - \lambda) \quad (12)$$

is the kinetic exponent. Thus, if the aggregation kinetics is mean field, z and λ are tied together, linking the kinetics and the resulting size distribution.

The great bulk of previous work concerning aggregation has assumed the cluster dilute limit, an assumption consistent with the mean field theory.[6,16] For systems with aggregates that diffuse between collisions and for which the rate of aggregation is thereby determined, the Brownian aggregation kernel holds with homogeneity $\lambda = 0$ to imply a kinetic exponent $z = 1$. Moreover the aggregates are fractal with a dimension of $D_f = 1.8$ and prefactor $k_0 = 1.3$.[17] This model of irreversible aggregation has been named diffusion limited cluster aggregation, DLCA, and is quite common.[5,18] Other models of irreversible aggregation are known including reaction limited cluster aggregation, RLCA, with $D_f = 2.1$ and ballistic limited cluster aggregation, BLCA, with $D_f = 1.9$. For all these $D_f < d$, so we now realize that with time the dilute condition will eventually break down. Thus we are led to question: what are the kinetics and what cluster morphologies appear in the cluster dense regime? These questions are resolved below.

3.2 Aggregation kinetics when dense

3.2.1 Simulations. Both on- and off-lattice, Monte Carlo diffusion-limited cluster–cluster simulations have been used to study the kinetics of aggregation in particulate systems as they evolve from the cluster dilute limit to the cluster dense regime and ultimately the gel point.[7–9,19–21] Results show that the kinetics become more rapid as the system evolves into the cluster dense regime as quantified by an increase in the kinetic exponent z. Enhanced aggregation rates in dense systems have also been observed with molecular dynamics calculations.[22,23] This is demonstrated in Fig. 2 which is a log–log plot of the normalized cluster mass as a function of aggregation time normalized by the gel time. According to eqn (11) such a plot has a slope of z. Initially, when a system is in the cluster dilute regime, the kinetic exponent is $z = 1.0$ as expected for a DLCA, Brownian aggregation kernel with $\lambda = 0$. But as a system evolves, z begins to increase, as shown by the increasing slope in Fig. 2. It has been shown[7] (see Fig. 5 below and the associated discussion) that this increase begins when the cluster occupied volume fraction enters the decade between 1 and 10% (hence on average about 3%) and reaches a value of $z = 2$ at the ideal gel point (cluster volume fraction of 100%).

To first-order the enhanced kinetics can be explained as due to the smaller amount of free volume available for the clusters, hence the larger effective cluster concentration, when the system becomes cluster dense.[7] This is demonstrated in Fig. 3 which plots the free volume corrected inverse number of clusters. The free volume corrected kinetics is now in rough accord with $z = 1$ for nearly another decade in time until it fails precipitously. The implication of this simple, first-order correction is that crowding

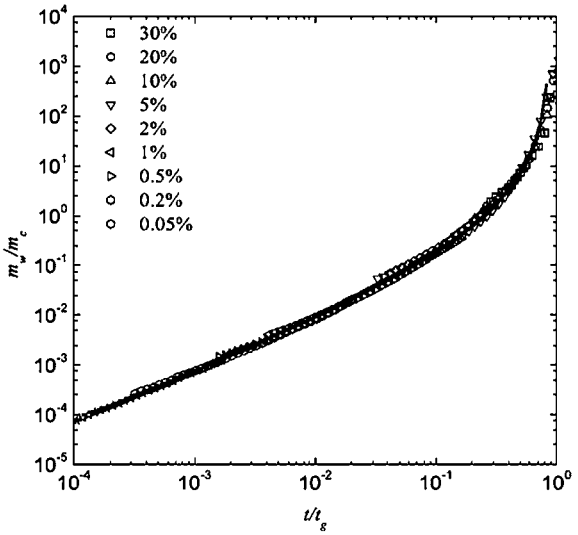

Fig. 2 Normalized cluster mass *versus* normalized aggregation time for different monomer volume fractions. Slope of this plot is the kinetic exponent z (from ref. 8).

is important. An important observation is that this correction breaks down when $f_{v,c} \approx 0.1$ equivalent to when $\lambda \approx 0.2$.

Gimel, Durand and Nicolai[20] first demonstrated the usefulness of the free volume for describing the progression towards the gel point. A polydispersity index, K, can be defined as

$$K = s_2/s_1 = (2 - \lambda)/(1 - \lambda). \quad (13)$$

K is a measure of the width of the aggregate size distribution. Gimel *et al.* simulated three dimensional, irreversible aggregation on a cubic lattice and showed that K increased from its dilute, DLCA limit value of $K = 2$ with increasing time of aggregation

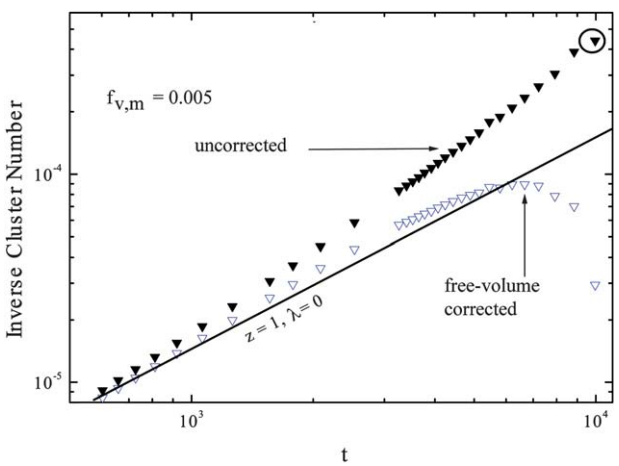

Fig. 3 Inverse cluster number *versus* time for 3d DLCA simulations with a monomer volume fraction of 0.005. Filled symbols (uncorrected) are the raw data from the simulation; note the increasing slope, hence the increasing exponent z, with time. Open symbols (corrected) have been corrected to account for the smaller free volume available to the clusters in this cluster dense regime. For reference a line of slope $z = 1$, the cluster dilute limit, is drawn. Large open circle marks the ideal gel point (from ref. 7).

with an apparent divergence near the gel point. Universal behavior, independent of the monomer volume fraction, was obtained by plotting K *versus* a function of the total effective volume V_{eff} of the aggregates. V_{eff} is related to $f_{\mathrm{v,c}}$ of eqn (5) but subtracts out cluster overlaps. Their results are given in Fig. 4, where a universal "critical phenomena-like" divergence is displayed.

The usefulness of free volume for describing the aggregation evolution is further illustrated in Fig. 5 which plots z determined from the kinetics, z_{kin} the dark symbols, as a function of the cluster volume fraction $f_{\mathrm{v,c}}$ for a variety of monomer volume fractions. All the data essentially fall together (relative to a plot of the same variables *versus* aggregation time, see ref. 7) to imply cluster volume fraction is a universal parameter for the aggregation process. Equivalent descriptions of this same universality can be obtained as functions of time with t/t_{g}, where t_{g} is any one of three gel times, see below, or $R/R_{\mathrm{g,G}}$.

The kinetics and the aggregate size distribution are closely tied together *via* eqn (12) for the mean-field SE. Fig. 4 and numerous other simulations have shown that the cluster size distribution broadens, as indicated by an increasing K, hence by eqn (13) an increasing λ, as the particulate system nears the gel point.[7–9,20,21] The parameter λ describes the size distribution *via* eqn (10), above, and is also the aggregation kernel homogeneity, eqn (8). Fig. 5 includes size distribution data in the form of $z_{\mathrm{sd}} = 1/(1-\lambda)$, open symbols. Two features are thereby displayed: First, the size distribution parameter is again demonstrated as a universal function of the cluster free volume. Second, the kinetic exponent z_{sd} derived from the size distribution parameter *via* the SE prediction $z_{\mathrm{sd}} = (1-\lambda)^{-1}$, eqn (12), is roughly equal to the z_{kin} obtained from the kinetics. This second fact implies that eqn (12) remains valid deep into the cluster dense regime, and since eqn (12) is a result of the mean-field SE, the mean-field assumption predictions must remain valid deep into the cluster dense regime as well.

Thus, surprisingly, the predictions of the SE, derived under cluster dilute assumptions, remains valid deep into the cluster dense regime right up to the ideal gel point where the cluster occupied volume is 100%! Mean field theory makes the assumption that the positions of the clusters are uncorrelated so that their collision probability is proportional to the square of the cluster number density. Fig. 6 shows cluster–cluster correlation functions from simulations deep in the cluster dense regime including the ideal gel point. There is only the anticorrelation due to mutual cluster exclusion; otherwise the correlation is within error featureless. This featureless correlation function is consistent with the previous conclusion that the mean-field SE accurately describes a dense system.

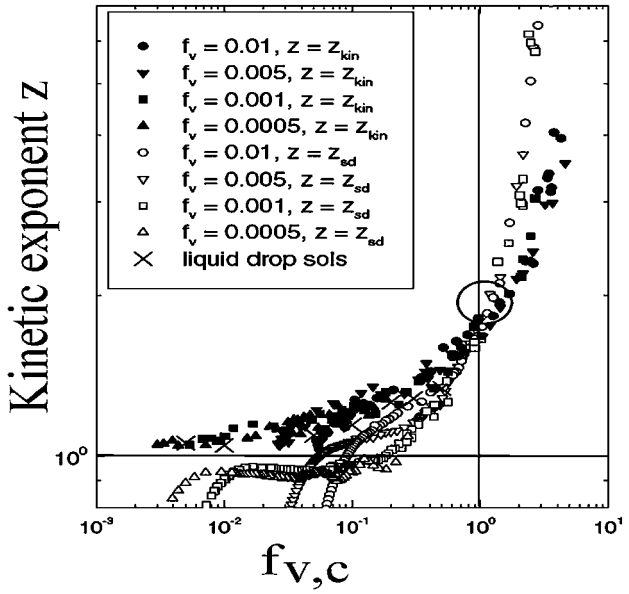

Fig. 5 The kinetic exponents z_{kin} obtained directly from the kinetics, closed symbols, and z_{sd} obtained from the size distribution determined value of λ *via* $z_{\mathrm{sd}} = (1-\lambda)^{-1}$, open symbols, plotted *versus* the cluster volume fraction $f_{\mathrm{v,c}}$. Large open circle marks the ideal gel point where $z = 2$. Results for liquid drop, coalescing sols are shown with X's (from ref. 7).

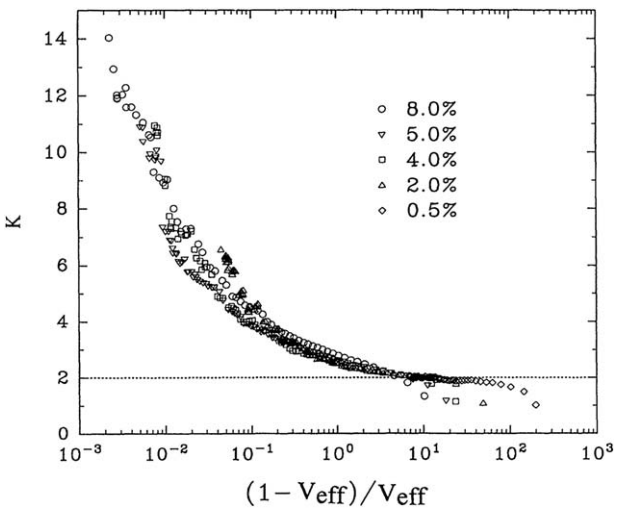

Fig. 4 Polydispersity index K evolution with the reduced cluster effective volume for a three-dimensional aggregation simulation with various monomer volume fractions. Note universality with the volume fraction (from ref. 20).

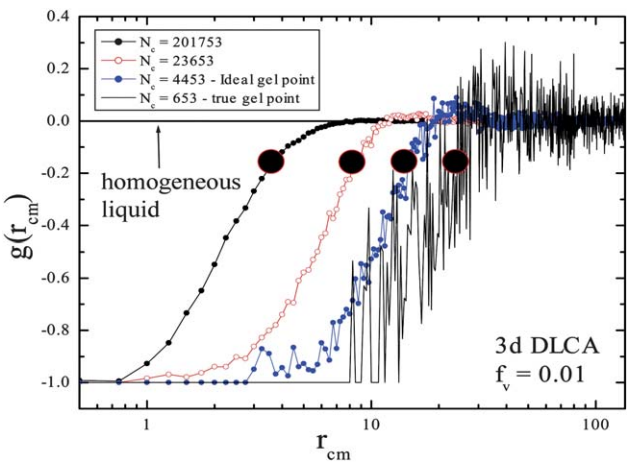

Fig. 6 Cluster–cluster spatial correlation function for 3d DLCA simulation at different times during the aggregation. The monomer volume fraction is 0.01. Large circles mark the mean cluster nearest neighbor separation $<R_{\mathrm{nn}}>$.

Regarding the validity of the SE for controlling the kinetics, recent work by Corezzi and coworkers[24–27] studied a loop-less aggregation process of ellipsoidal, patchy particles with off-lattice simulations. They compared their numerical results with SE predictions and found very good agreement up to (and even a little above) the ideal gel point.

Some reservation is warranted here. Ziff *et al.*[28] have pointed out that even if the predictions of the SE are valid, it does not necessarily follow that the equation itself is valid. However, given that the predictions of SE hold and that there are no significant correlations in the density, the argument for SE validity has some merit even if it falls short of proof. Despite this caveat, these results imply that the predictions of the SE can be used to describe the aggregation from the dilute to the dense and up to the ideal gel point. Furthermore, it appears that the cluster dense nature of the system does not destroy the SE but instead increases the homogeneity λ of the aggregation kernel. This latter concept will be supported by theoretical analysis below.

Returning to Fig. 5, we observe that λ and z evolve in parallel up to the ideal gel point, where $\lambda = 0.5$, $z = 2$. Beyond the ideal gel point, z_{sd} becomes larger than z_{kin} but each remains universally related to the free volume, which is now negative, indicating interdigitation of aggregates. This behavior continues up to the presence of the first system spanning cluster, the "true" or physical gel point, and finally the end of aggregation as the system becomes static. The inequality of exponents implies that mean-field SE theory does indeed break down beyond the ideal gel point.

A test of the importance of the free volume that eliminates the ramified, fractal nature of the gelling aggregates can be made by simulating the coalescence of liquid droplets which, because of their compact geometry, do not change in total cluster volume with continued aggregation. Fig. 5 shows that these yielded z_{kin} values are in agreement with the non-coalescing particles strongly supporting the contention that crowding is the only factor for enhanced kinetics. Cluster morphology, fractal or dense, and impending gelation are of no consequence.

Simple scaling arguments can be invoked to calculate the kernel homogeneity in limiting cases.[7,29] These scaling arguments make use of the length scales R_g and R_{nn} that were used in the simple explanations of gelation surrounding Fig. 1, above. These length scales account for the increasing proximity of the clusters as the cluster volume fraction increases. The aggregation kernel, K, is the rate at which two clusters collide. This is proportional to their relative cross-sectional area A and relative velocity, v, yielding $K \sim Av$, which has the correct units. In the dilute limit, R_g is the only relevant length scale in the system. Thus, for Brownian diffusion $v \sim D/R_g$, where D is the diffusion coefficient, giving $K \sim DR_g$, originally derived by Smoluchowski.[12] Since $D \sim 1/R_g$, K is constant and $\lambda = 0$. As the system continuously gets crowded, R_{nn} eventually becomes a relevant length scale with respect to any given cluster's motion. When that happens, at some intermediate time regime, one can estimate the characteristic velocity as $v \sim D/R_{nn}$. This makes $K \sim N^{0.22}$, hence $\lambda = 0.22$ consistent with simulation results in the intermediate regime.

A characteristic of cluster dilute aggregation is that any two neighboring clusters can collide at any relative direction regardless of their initial separation direction. However, as the system transforms from cluster dilute to cluster dense, the direction of approach for two clusters evolves from this isotropic situation to uniaxial along the line separating their centers. Thus at the ideal gel point, the overall motion is "ballistic-like" since any cluster motion prior to a collision is effectively along this line and small relative to the cluster size. The effective cluster velocity is then given through the equipartition of energy as $v \sim N^{-1/2}$. In such a crowded state, a cluster sees the "fingerlike" detail of a neighboring fractal aggregate and the cross-sectional area must be replaced by the surface area which for a fractal is proportional to N. Thus, the kernel crosses over to $K \sim N^{1/2}$, yielding $\lambda = 0.5$ in agreement with the simulation results at the ideal gel point. This scaling argument is summarized in Table 1.

With this scaling argument, recall the breakdown of the simple, first-order correction for the free volume in the system, shown in Fig. 3, which occurred at $\lambda \approx 0.2$. Scaling predicts this value when the nearest neighbor spacing becomes a relevant parameter, *i.e.*, crowding effects the free volume. Larger values of λ occur, according to scaling, due to the increasing likelihood of ballistic motion between cluster collisions. Thus the breakdown of simple free volume correction at $\lambda \approx 0.22$ is consistent with scaling and demarks a boundary between free volume affects at earlier times and ballistic effects at later times, both within the cluster dense regime.

Table 1 Scaling Predictions for the aggregation kernel K, kernel homogeneity λ, and kinetic exponent z

Regime	Length Scale/s	Kernel, $K \sim vA$	Exponents λ, z
Dilute	R_g	$\left.\begin{matrix} v \sim D/R_g \\ A \sim R_g^2 \end{matrix}\right\} K \sim DR_g \sim R_g^0 \sim N^0$	$\lambda = 0$ $z = 1$
Dense	$R_g \sim N^{1/D_f}$ $R_{nn} \sim N^{1/d}$	$\left.\begin{matrix} v \sim D/R_{nn} \\ A \sim R_g^2 \end{matrix}\right\} K \sim \frac{DR_g^2}{R_{nn}} \sim \frac{R_g}{R_{nn}} \sim N^{1/D-1/d}$	$\lambda = \frac{d-D}{dD} \simeq 0.22$ $z = \frac{dD}{dD-d+D} \simeq 1.29$
Ideal Gel Point	Cluster Surface Separation $\ll R_g, R_{nn}$	$\left.\begin{matrix} v \sim (kT/N)^{1/2} \\ A \sim N \end{matrix}\right\} K \sim N^{-1/2}N \sim N^{1/2}$	$\lambda = 1/2$ $z = 2$

Past the ideal gel point, mean field, SE kinetics breaks down. The parameter λ is now more appropriately called the scaling exponent, eqn (10), rather than the aggregation kernel homogeneity, because with an invalid SE, what does it mean to define an aggregation kernel? In this regime simulations tell an ambiguous story with λ increasing continuously above 0.5 to *ca.* 0.9, but also some evidence for $\lambda = 2.2$ near the physical gel point.[7,8,22] This latter value is that predicted from static percolation theory. How λ might evolve from 0.9 to 2.2 has not been discovered.

3.2.2 Experiments. Experiment has for the most part ignored dense sol kinetics, but some data do exist. Carpineti and Giglio[30] reported enhanced kinetics at late times during salt induced aggregation of a polystyrene microsphere colloid. Dhaubhadel[31] reanalyzed their data to find the kinetic exponent z to increase from 1.3 to 2.3, with considerable uncertainty, for some of their data, giving some support to the notion of increasing z with cluster density. Experiments in our laboratory showed enhanced aggregation kinetics in a dense soot aerosol in a heavily sooting flame.[32] The flame was a simple Bunsen burner configuration to create a laminar acetylene (C_2H_2)/air diffusion flame. At large acetylene gas flow rates, the soot, as seen *via* microsecond photographs, forms a remarkable, continuous network across the annular flame front, see Fig. 7. This is an explicit demonstration of gelation in an unlikely environment. Semi-quantitative measurements showed the aggregation rate was *ca.* 460 times faster than that expected for the soot number density and flame conditions.

Wu, Xie and Morbidelli[33] studied the aggregation kinetics of an aqueous suspension of a denatured whey protein isolate with monomer diameter of 32.5 nm. These formed $D_f = 1.85$ fractal aggregates. Kinetic data, shown in Fig. 8, were obtained *via* static light scattering after the aggregates had a radius of gyration of $R_g \approx 1000$ nm and larger. The similarity between these results and the simulations of Rottereau *et al.*,[8] shown in Fig. 2 is startling, and indeed Wu *et al.* were able to fit their data to the simulations. In the region 1000 nm < R_g < 10,000 nm R_g was seen to increase at an enhanced rate relative to the value expected for the dilute regime. Analysis of these data yields a kinetic exponent

Fig. 7 Microsecond photograph of a soot gel 10 cm above the opening of a Bunsen-type burner in a laminar acetylene flame in air.

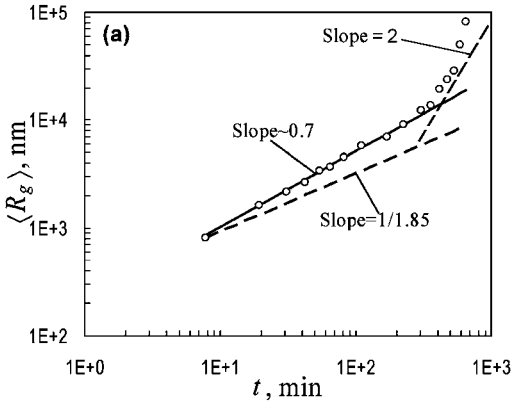

Fig. 8 Time evolution of the average radius of gyration of clusters forming from an aggregating colloid of 65 nm diameter whey protein isolate monomers. Note the similarity to Fig. 2. A slope of the inverse of the fractal dimension, 1/1.85 for these aggregates, is expected in the cluster dilute, DLCA regime. A slope of 2 is expected as the system passes through the ideal gel point (adapted from ref. 33).

of $z = 1.29$, in good agreement with the dense regime scaling predictions in Table 1, which for $D_f = 1.85$ yield $z = 1.26$. For yet larger R_g the effective z exponent continues to increase, as predicted by Fig. 5.

Recently our laboratory studied the aggregation kinetics of a soot aerosol confined to a disk shape volume.[34] The volume was 51 mm in diameter and 10 mm thick although provisions could be made to decrease the thickness of a portion of the disk to lessen the effects of multiple light scattering. A carbonaceous soot aerosol was created in this volume by filling it with a mixture of acetylene and oxygen and then exploding this mixture with an electric spark. The soot particles were roughly spherical with a radius of *ca.* 38 nm as determined by transmission electron microscopy of samples extracted from the volume. Monomer volume fractions were 1 to 10 $\times$ 10^{-5} as determined by light scattering/extinction measurements. The end of the rapid explosion (*ca.* 30 ms) marks the beginning of the physical aggregation process for the soot aerosol which gelled on the order of 100 s depending on the monomer volume fraction.

The aggregation kinetics was watched by small angle static light scattering. This technique allowed for measurement of the aggregate mean R_g and D_f. The circular disk walls were flat glass windows. Optical structure factors, scattered intensity *versus* scattering wave vector,[35] were measure with 1 s resolution. Corrections for multiple scattering were made. Plots of R_g *versus* time yielded z/D_f; D_f was obtained independently from the optical structure factor; thus z was measured.

The results of these experiments are shown in Fig. 9 were both the kinetic exponent z and the kernel homogeneity λ, calculated simply from eqn (12), $\lambda = 1 - z^{-1}$, are plotted *versus* monomer volume fractions. Different monomer volume fractions are different experimental runs.

Fig. 9 shows that the kinetic exponent increases uniformly from the cluster dilute, DLCA limit of $z = 1$ for small monomer volume fractions to 1.9 at large monomer volume fractions. The smaller monomer volume fractions barely gelled before gravitational settling ruined the experiment. The largest monomer volume fraction runs gelled so fast that the time resolution of 1 s

was barely able to resolve the aggregation. Thus the experiment could not resolve the evolution of the exponent z as the cluster volume fraction evolved for any single run and the z values represent averages over the entire run. Regardless of this limitation, the results are completely consistent with the simulation results above that the onset of cluster crowding as an aggregating system enters the cluster dilute regime is described by the increase in the kinetic exponent z from 1 to 2.

Dhaubhadel *et al.*[34] also measured the overall rate of the aggregation and found it to be *ca.* an order of magnitude larger than expected from Brownian dynamics. This is consistent with earlier results but has not been studied further with simulation or theory.

3.2.3 The gel times. An important kinetics question is: given the initial conditions of a sol, how long after it is destabilized will it gel? To begin to answer this one can apply the concept of the ideal gel point to a DLCA system and assume that DLCA kinetics applies up to the gel point.[36] We now know that this latter assumption fails significantly so our result will yield a time too slow. Nevertheless, the result will be useful.

To order unity the "mass" of the aggregates at the ideal gel point is from eqn (1) and (6)

$$N_G \approx f^{(D_f/(D_f-3))}{}_{v,m} \tag{14}$$

The SE can be written in a simple form under the assumptions of a constant kernel and same sized aggregates as

$$dn/dt = -Kn^2 \tag{15}$$

With solution

$$n = (Kt)^{-1} \tag{16}$$

From conservation of mass, $N_c = N_m/N$. Moreover, the monomer volume fraction is approximately $f_{v,m} \approx N_m a^3/V$. Recall $n = N_c/V$. Then combining these relations with eqn (14) and (16) yields an expression for the gel time

$$t_G \approx K^{-1} a^3 f_{v,m}{}^{-3/(3-D_f)} \tag{17}$$

For DLCA with $D_f = 1.8$ this becomes

$$t_G \approx K^{-1} a^3 f_{v,m}{}^{-2.5} \tag{18}$$

The power law on the volume fraction has been amply demonstrated as true in simulations. On the other hand the magnitude has not been tested.

The result in eqn (18) is very instructive. It shows that if the monomers are small and their volume fraction is large, *i.e.*, *if there is a lot of finely divided matter*, the system will gel quickly.‡ Moreover, the functionalities are very strong. Fig. 10 shows plots of eqn (18) for both a colloidal system in water and an aerosol system in air both at room temperature. With the assumptions made above in mind, Fig. 10 shows that experimentally accessible gelation times can be obtained for nanoscale systems of appreciable but not necessarily extreme density. A revelation in our laboratory was that aerosols can gel provided the gel time was faster than other characteristic times for the system such as settling times and wall deposition times.[32,36]

‡ We recall gelatinous precipitates such as "$Fe(OH)_3$" formed by the addition of NH_4OH to aqueous Fe^{3+} at high concentration. The very small solubility product of the "$Fe(OH)_3$" causes an extreme supersaturation, which in turn causes a very fine precipitate. This highly concentrated, very fine precipitate leads to, by our argument, a quickly forming gel.

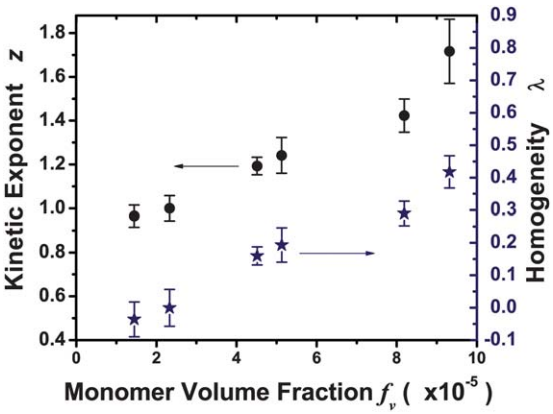

Fig. 9 Experimental kinetic exponent and inferred kernel homogeneity for different monomer volume fractions of gelling soot aerosols (from ref. 34).

Simulations indicate that the process of gelation has several "gel times".[8,21] First to occur is the ideal gel point where the cluster volume fraction goes to one and which scales as described in eqn (17) and (18). Next follows the true or physical gel point when the first, system-volume-spanning cluster forms. Empirical results from simulations indicate $t_g \approx 3t_G$.[21] After that, the remaining clusters, lattice animals, attach to the spanning cluster until there is only one grand cluster, the gel, the final state at t_f. Empirical results from these simulations indicate $t_f \approx 8t_g \approx 24t_G$.[8]

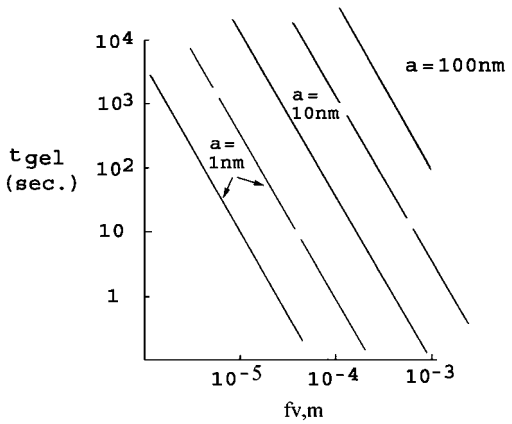

Fig. 10 Gel times calculated under the assumption of cluster dilute kinetics for different monomer radii a as a function of the monomer volume fraction. Solid lines are for aerosols in air, dashed line for colloids in water, both at $T = 20$ °C and atmospheric pressure (adapted from ref. 36).

4 Aggregate morphology near the sol–gel transition

4.1 The cluster dilute limit

It is now well established that when solid particles come together to form aggregates *via* random Brownian motion the result is a fractal morphology. The most common forms of aggregation are DLCA and RLCA, mentioned above, involving aggregates random walking, meeting and sticking together with either high or low probability, respectively. In three dimensional space DLCA leads to fractal aggregates with $D_f = 1.78 \pm 0.1$ and $k_0 = 1.3 \pm 0.2$. These numbers can be considered universal since results from a wealth of simulations,[5,17,18,37,38] experiments on both aerosols and colloids[6,15,16] and a simple analytical theory[39] all concur. Simulations for RLCA lead to $D_f = 2.1 \pm 0.1$ and $k_0 = 0.94$.[40]

4.2 The cluster dense regime

From our present perspective we now see that these classic results apply to particulate systems in the cluster dilute regime. In this regime the clusters are so far apart that the relative diffusive random walk of any two clusters allows them to collide with each other randomly from any direction. As the system becomes cluster dense, however, the directions of collisions are no longer isotropic. In a cluster dense state a cluster to the right of a given cluster will more likely collide from the right and so on. The question then arises: how, if at all, does this anisotropy of collisions induced in the cluster dense state change the resulting aggregate morphology?

4.2.1 Simulations. This question has been addressed with simulations. Hasmy and Jullien[41] simulated 2d systems of high monomer volume fractions and saw the canonical DLCA result of $D_f = 1.44$ early in the aggregation process crossover to $D_f = 1.9$, the static percolation result for 2d, late in the aggregation process. Gimel and coworkers[8,9,21] simulated 3d systems with a broad range of monomer volume fractions from 0.0005 to 0.3. They found a crossover in the scaling of mass *versus* the linear size form fractal dimensions of 1.8 at small size to 2.5 at large. This latter dimension is essentially equal to the dimension of a percolation cluster, 2.55. Thus it was concluded that when the clusters became large and hence the system entered the cluster dense regime, the clusters developed a percolation morphology.

Our group addressed this question with 3d off-lattice, Monte Carlo simulations that were large enough to allow observation of the crossover from cluster dilute to dense for DLCA, RLCA and BLCA.[11] Monomer volume fractions ranged from 0.0005 to 0.1 with system sizes up to 580 monomer diameters cubed. The structure of the resulting aggregates was investigated with both real and reciprocal space analyses. The real space analysis involved the method of nested spheres wherein the scaling of the mass within spheres centered on the aggregate with the radius of the spheres yields the fractal dimension. The reciprocal space analysis involves calculating the Fourier transform, squared, $I(q)$ of the system or aggregate and looking for its possible scaling with q as $I(q) \sim q^{-D_f}$. $I(q)$ is the structure factor of the object. This method simulates a wave scattering experiment (*e.g.*, light) from the object.

Fig. 11 displays the evolution of the DLCA structure factor for the *largest* cluster in the system with a monomer volume fraction of $f_{v,m} = 0.01$. Early in the aggregation a $q^{-1.78}$ power-law regime is seen to imply the canonical DLCA aggregate structure with $D_f = 1.78$. There are also a q-independent Rayleigh regime at the smallest q and the transition between these two regimes, the Guinier regime, which indicates the aggregate size, $R_g \approx q^{-1}$ at the transition. This Guinier transition evolves to smaller q as the system aggregates. Of significance is that late in the aggregation run the aggregate power-law regime develops a second slope of ≈ 2.6 indicating a different fractal dimension at smaller q hence larger length scales.

These results can be interpreted to imply that late in the DLCA aggregation process the largest aggregate in the system has an inhomogeneous, hybrid structure described by a short-range *local* structure with a fractal dimension of $D_f \approx 1.8$ and a long-range *overall* structure with a fractal dimension of $D_f \approx 2.6$. We call such a structure a "superaggregate" because it is an aggregate with an overall fractal dimension that is composed of smaller aggregates with a different fractal dimension.[11] A proposed picture of a superaggregate is drawn in Fig. 12.

Crossovers of slope on a log–log plot of a structure factor occur at characteristic length scales of the object. Thus the crossover between the two fractal power-laws in Fig.11 implies a length scale for the superaggregate. This crossover length scale matches very well with the inverse of the radius of gyration at the ideal gel point, $R_{g,G}$, given by eqn (6) as indicated by the arrow.

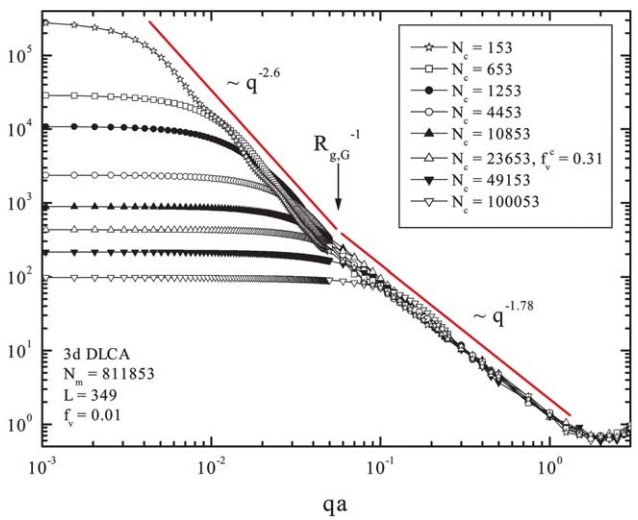

Fig. 11 Structure factor $I(q)$ of the largest cluster at different times during aggregation for a three-dimensional DLCA simulation with a monomer volume fraction $f_{v,m} = 0.01$. Here N_c is the number of clusters at a given time during aggregation. Thus, smaller N_c corresponds to a later time. The location of the calculated ideal gel point radius of gyration is shown as $R_{g,G}^{-1}$. Early in aggregation a $q^{-1.78}$ power law is observed characteristic of a DLCA aggregate with a fractal dimension of $D_f = 1.78$. Near the gel point, $I(q)$ evolves to show two power-law regimes. The $q^{-1.78}$ functionality mentioned above remains intact, but at smaller q, hence at a larger length scale, a $D_f = 2.6$ regime appears. For yet smaller values of q, the power law gives way to a q-independent Rayleigh regime (from ref. 11).

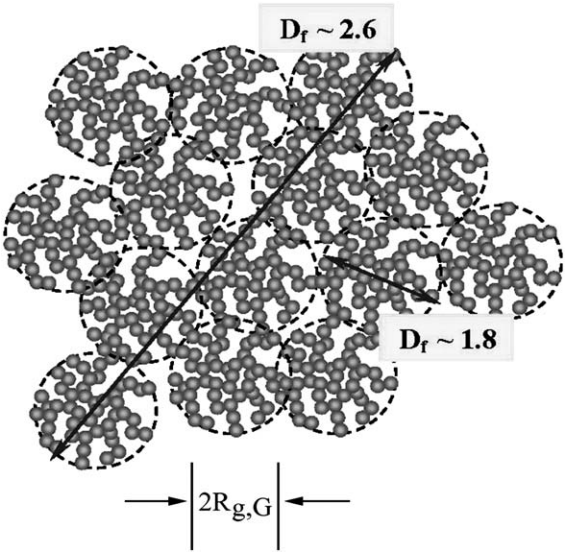

Fig. 12 Conception of a superaggregate.

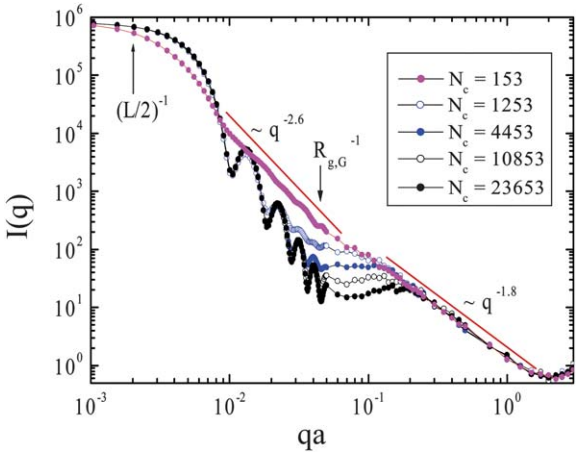

Fig. 13 Structure factor of the entire system at different times after the onset of aggregation for a three-dimensional off-lattice simulation with a monomer volume fraction of 0.01. $R_{g,G}$ is the ideal gel point radius of gyration; N_c is the number of clusters in the system, which decreases with increasing time; and L is the system box size (adapted from ref. 42 and 43).

This correspondence between the crossover and the $R_{g,G}$ value was explored over a wide range of monomer volume fractions and fractal dimensions (*via* the RLCA and BLCA aggregation models) and proved to hold very well. However, the RLCA and BLCA aggregation models yielded less distinct crossovers. This is very likely due to the greater aggregate polydispersity that results from these two models. Regardless, the similarity implies a universality for what might be termed the "ideal gel point transition". This universality follows from the scaling analysis for the aggregation kernel above. That analysis argued that as the system approached the ideal gel point, the motion between cluster collisions became ballistic, regardless of the cluster dilute motion. Recall that this argument successfully predicted a kernel homogeneity of $\lambda = 0.5$.

The structure factor for the entire gelling system is shown in Fig. 13.[42,43] In contrast to Fig. 11 the evolution displayed there is that which might be visible in a scattering experiment. At early times, which corresponds to a large number of clusters N_c, the canonical $q^{-1.8}$ regime is seen at large q characteristic of $D_f = 1.8$ fractal aggregates. At small q the structure factor of the system box is seen with characteristic size L and a Porod regime with q^{-4} envelope over interference ripples. Between these two lies a small peak. With time, the peak disappears as the scattering below the peak rotates or shifts upward. This upward shift eventually affects the system Porod regime by eliminating the ripples and reducing the slope to imply a power law of $q^{-2.6}$, as indicated.

This result is consistent with the prediction of the scaling description of scattering presented by Oh and Sorensen.[44] The peak in the structure factor has been seen in a number of dense aggregating colloids since it was first observed by Carpeneti and Giglio.[30] It has garnered considerable attention and is often, and we claim erroneously, interpreted to imply a fundamental length scale of the system. In fact, this peak can be shown to be the result of how two length scales R_g and R_{nn} affect the structure factor.[44–46] When they approach one another near the gel point, as illustrated in Fig. 1, they combine to yield a peak if the aggregate size distribution is not too polydisperse. This restriction on polydispersity holds for DLCA but not RLCA, so only a weak or no peak is seen with RLCA. Note that once again R_g and R_{nn} are the important length scales for describing phenomena near the gel point.

The shift of the plot upward for q less than the peak can be interpreted as due to the onset of fractal aggregates with dimension $D_f = 2.6$ in the length scale range greater than $R_{g,G}$. At some yet larger length scale, these superaggregates are limited in size but are bound together in a gel that appears homogeneous at and beyond this very large scale. Then by ref. 44 we predict that a q^{-4} power law would appear and continue with decreasing q down to the inverse of the size of the entire gel.

This pleasing interpretation requires further study before it can be completely accepted. The length scales L and $R_{g,G}$ are only a factor of 25 different and so finite size effects might be involved in the appearance of the −2.6 slope in Fig. 13. Rottereau *et al.*[9] have shown that the entire system displays a correlation length that is essentially the mean size of the aggregates in the cluster dilute regime. This correlation length increases with the aggregation but levels off to the $R_{g,G}$ value as the system passes through the ideal gel point on to the final state. For length scales greater than the correlation length, the system is homogeneous and three dimensional. Then the −2.6 slope would not appear in the structure factor of the entire system, but only when individual clusters are studied separately as in Fig. 11.

4.2.2 Experiment. A number of light scattering experiments on gelling colloids have appeared through the years. They can be classified as those displaying a simple power law of the scattered intensity *versus* scattering wave vector and those that show a peak in the scattered intensity. Examples can be found in ref. 47, and 30 and 48, respectively. These features correlate with aggregation in the RLCA regime or the DLCA regime, respectively. The peak only occurs when the system has evolved *via* DLCA to be near the gel point. None of these early experiments have shown a hybrid, superaggregate structure, but none had a q range that sufficiently overlapped with the $R_{g,G}$ that we can now

calculate. At present it appears that clusters with a super-aggregate morphology have been observed in three different experiments: soot aerosols in flames, a gelling colloid, and a sheared, gelling colloid.

Laminar, diffusion flames of heavily sooting fuels exhibit gelation of the soot aerosol in the flame.[32,43,49,50] The gel network in an acetylene flame was shown in Fig. 7, above, and static light scattering data for this flame are shown in Fig. 14.[43] Soot in a flame forms, to first order, in a two step process. First a complex chemistry ensues to convert the fuel into roughly spherical carbonaceous particles with diameters of about $2a \approx$ 30 to 60 nm. Subsequently, and for the most part independently, these monomeric particles aggregate *via* DLCA. Fig. 14 shows that for the acetylene flame at small heights above the burner, which represents short aggregation times for the soot, submicron $D_f \approx 1.8$ aggregates of soot formed. This is a well known result for sooting flames. Remarkably, with increasing height above the burner a second feature in the scattering develops at low q, thus large length scales. This low q feature has the signature of *ca.* 10 micron aggregates with a fractal dimension of $D_f \approx 2.6$ for the length scale range 1 to 10 microns. Overall, the data at large heights, hence large aggregation times, indicates superaggregates of soot with $D_f \approx 2.6/1.8$ large scale/small scale morphologies. Subsequent work found soot superaggregates in flames of other heavily sooting fuels (typically unsaturated hydrocarbons with large C/H ratios).[43,49,50]

These results are consistent with the simulations of Fry *et al.*[11] described above. Moreover, there is considerable similarity to the theoretical structure factor of Fig. 13 for both the shape of the curve and the position of $R_{g,G}$, which was calculated for the flame soot aerosol. However, the shape of the experimental curve does appear to have a longer plateau region between the two power laws.

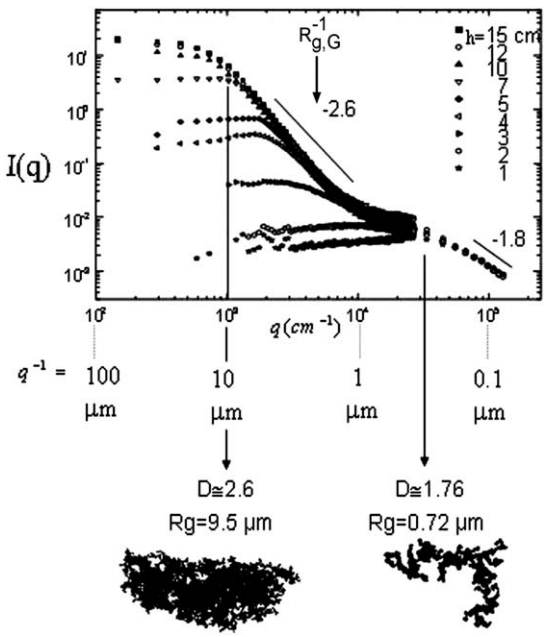

Fig. 14 Light scattering static structure factor of a soot aerosol in a laminar diffusion acetylene flame from a Bunsen-type burner. Height above the burner orifice is designated by h and larger values lead to longer aggregation times for the soot aerosol. With increasing h, the $D_f = 2.6/1.8$ superaggregates appear. Below are electron microscope pictures of soot captured from the same flame with values of R_g and D_f determined from the analysis of the micrographs, values in good agreement with the light scattering results (From ref. 50).

Fig. 14 also includes examples of soot sampled from the flame *via* thermophoresis. Transmission electron micrograph analysis yielded sizes and fractal dimensions consistent with the light scattering analyses. This is an important reassurance since the large size and large, complex refractive index of the soot super-aggregates makes the Rayleigh–Debye–Gans assumption of the light scattering analysis uncertain.

We have found that a simple laminar diffusion flame, in essence a Bunsen burner, can lead to very complex soot morphologies as a consequence of aggregation and gelation. The annular flame front between the inner cylinder of flowing fuel as it exits from the cylindrical burner and the surrounding air can grow very thin while the 3d superaggregates grow large. This happens to the point where the superaggregates find themselves in a 2d space in the relatively "flat" flame front. Then 2d DLCA ensues[51] and eventually 2d percolation to millimetre sized soot (five orders of magnitude larger than the monomers). The result is $D_f \approx 1.9/1.4/2.6/1.8$ corresponding to, with decreasing length scale, 2d-percolation/2d-DLCA/3d-percolation/3d-DLCA supersupersuperaggregates.[50]

We have also observed the $D_f \approx 2.6/1.8$ superaggregate morphology in soot aerosols created in a large 17 liter chamber.[52] The soot was collected late in the aggregation process *via* gravitational settling onto TEM grids inserted into the chamber. TEM and optical microscopy over length scales ranging from 100 nm to 100 microns showed $D_f = 1.8$ structure at smaller length scales < 1 micron and $D_f = 2.5$ structure at larger length scales.

Wu *et al.*[53] gelled colloids of nanospheres of a MFA latex with primary particle size of 37.5 nm radius and volume fractions of 2, 4, and 8%. These particles have the advantage that they have a low optical contrast with water; hence multiple scattering effects are minimized. Their static light scattering measurements, reproduced here in Fig. 15, show curves similar to Fig. 13 and 14. Wu *et al.* interpreted these curves using a structure factor derived by Wong and Cao[54] based on a surface fractal with dimension that varied from 2.45 to 2.82 enclosing a mass fractal that varied from 1.8 to 1.4, with increasing monomer volume fraction. A good fit was obtained. However, we propose that the similarity to Fig. 13 and 14 is compelling hence the superaggregate interpretation of their results is at least equally viable. We have calculated $R_{g,G}$ values and included these in Fig. 15 Here we see that whereas inverse $R_{g,G}$ values are near the plateau, they are on the large q side rather than the small q side, as predicted by Fig. 13.

Superaggregates with $D_f \approx 2.6/1.8$ have also been observed in sheared colloids.[55] The colloid was a $2a = 20$ nm diameter polystyrene colloid in water at a monomer volume fraction of 4.36×10^{-4}. This colloid could be destabilized with addition of an ionic salt into DLCA and would gel in *ca.* 50 min. Small angle light scattering was performed during the entire aggregation to gelation without shear and only $D_f \approx 1.8$ aggregate morphology was seen. The ideal gel point radius of gyration for this system is $R_{g,G} = 3000$ nm, hence $R_{g,G}^{-1} = 3000$ cm^{-1}, within the range of q values probed. This is at variance with the simulation prediction of Fig. 13 that a $q^{-2.6}$ regime should have been observed.

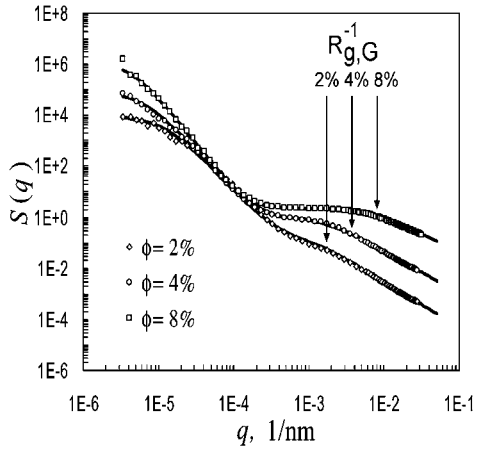

Fig. 15 Light scattering static structure factor of a gelling colloid of $a =$ 37.5 nm radius spheres with three different monomer volume fractions, $\varphi = f_{v,m}$. Values of the inverse ideal gel point radius of gyration, $R_{g,G}$, are indicated (adapted from ref. 53).

However, it is consistent with the experimental results of Wu *et al.*,[53] Fig. 15, that the $q^{-2.6}$ regime doesn't start to well below $R_{g,G}{}^{-1}$. On the other hand, if the system was sheared briefly for 30 s at various times after the start of aggregation due to the destabilization, $D_f \approx 2.6/1.8$ (nominally) superaggregates were observed, as shown in Fig. 16. It could be demonstrated that the appearance of the large $D_f \approx 2.6$ fractal dimension was not due to aggregate restructuring, often observed under shear. Instead it was shown that the shear caused an increase in size indicating that the $D_f = 1.8$ aggregates formed by DLCA were "super-aggregated" by the shear when the system was cluster dense.

In summary, there are only a few experiments on irreversible, gelling systems that have probed to small enough q to see structures beyond the normal DLCA fractal aggregates with $D_f = 1.8$. All of these are consistent with the proposition that $D_f \approx 2.6/1.8$ superaggregates form in aggregating systems near the gel point, but the possibility of a surface fractal enclosed mass fractal cannot be ruled out. The superaggregate description is supported by soot clusters retrieved from heavily sooting flames and simulations. Moreover that interpretation includes the ideal gel point radius of gyration length scale and calculated values yield semi-quantitative agreement with experiment. Certainly opportunity exists to explore systematically in greater detail the gelation of particulate systems.

5 Concluding remarks

We rejoin our introductory remarks. Irreversible particulate systems gel when their particles do not coalesce during aggregation but instead form ramified aggregates with a fractal dimension less than the spatial dimension, $D_f < d$. With the review above, we see that this causes the volume occupied by the clusters to increase with time until the entire system volume is consumed. This is the ideal gel point. The consequences of this increasing volume fraction are illustrated in Fig. 17 where the aggregation kernel homogeneity λ is plotted *versus* both the cluster volume fraction and the concomitant ratio of the mean cluster nearest neighbor distance to the cluster size, R_{nn}/R_g.

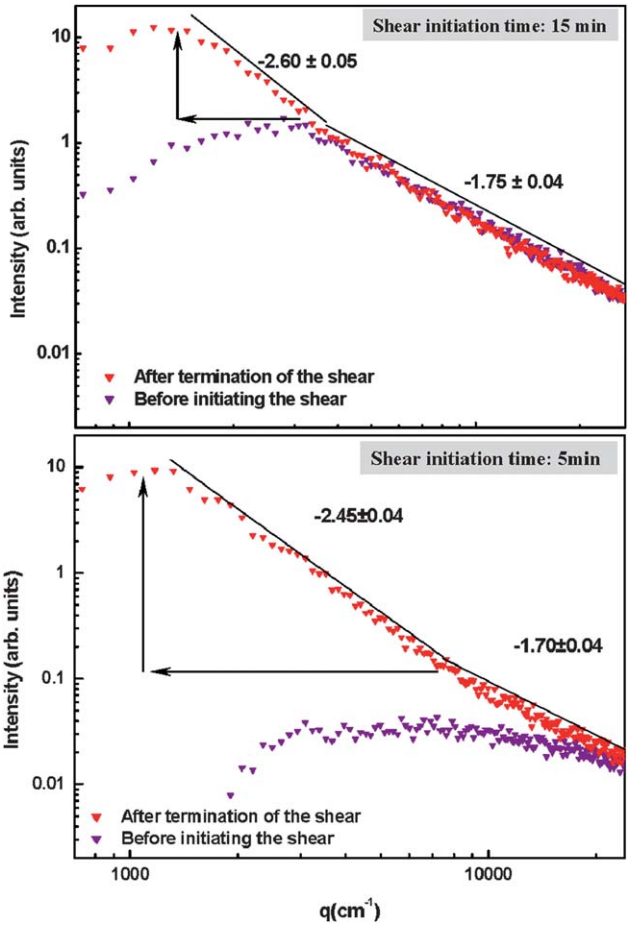

Fig. 16 Light scattering structure factor of an aggregating colloid of 20 nm diameter spheres with a monomer volume fraction of 4.36×10^{-4}. Shear was applied to the colloid at the shear initiation time after the colloid was destabilized for Brownian aggregation. The shears, 3.56 s^{-1} and 0.48 s^{-1} for (a) and (b), respectively, were applied for 30 s. Before the shear, canonical DLCA with $D_f \approx 1.75$ was observed. The shear caused aggregation to larger sizes with $D_f \approx 2.5/1.75$ superaggregate structure as indicated by the arrows (from ref. 55).

There we see that the homogeneity begins to increase from the cluster dilute limit value for DLCA of $\lambda = 0$ near $f_{v,c} \approx 10^{-3}$. This marks the approximate boundary between cluster dilute and cluster dense regimes. During the early stage of the cluster dense regime the motion of the aggregates is still diffusive between collisions and a simple free volume correction to the Smoluchowski equation will describe the aggregation kinetics. This implies that cluster crowding is the only factor changing the aggregation process relative to cluster dilute DLCA. In past work we have called this the intermediate regime. Near $f_{v,c} \approx 0.1$, when $\lambda \approx 0.22$, a new phase of the cluster dense regime is entered wherein, although the motion is diffusive, it is ballistic-like because the clusters collide along directions that increasingly coincide with their separation direction; *i.e.* the approach direction is no longer random but directional. This pre-gel ballistic regime drives the homogeneity to $\lambda = 0.5$. Up to this point the resulting morphology of the aggregates is equivalent to the canonical DLCA with homogeneous fractal structure and a dimension of $D_f = 1.8$. The end of the pre-gel-ballistic phase of

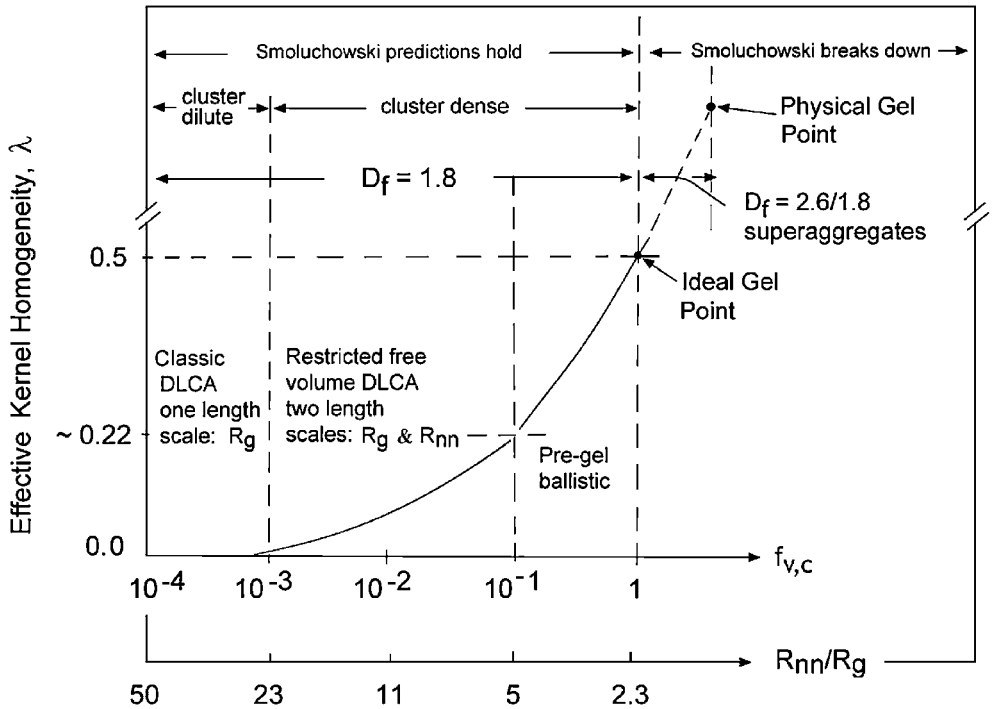

Fig. 17 The aggregation kernel homogeneity λ plotted *versus* the cluster volume fraction and the corresponding ratio of the mean cluster nearest neighbor distance to cluster size, R_{nn}/R_g. Various regimes, sub-regimes and important points are indicated.

the cluster dense regime is the ideal gel point at $f_{v,c} = 1.0$ ($R_{nn}/R_g = 2.3$). At and after the ideal gel point, the $D_f = 1.8$ aggregates act like monomers in a dynamic percolation process that yields $D_f \approx 2.6/1.8$ superaggregates. The crossover length scale between the $D_f = 1.8$ and 2.6 regions in the superaggregate is $R_{g,G}$ the radius of gyration at the ideal gel point. Thereafter, the remaining aggregates and superaggregates combine to form first a volume spanning aggregate and then a completely connected, single cluster entity that is the gel. These last stages past the ideal gel point are yet to be elucidated.

6 Acknowledgement

We thank our former students and post-docs J. Cerda, R. Dhaubhadel, D. Fry, C. Gerving, E. Gilbertson, W. Hageman, H. Huang, W. Kim, T. Mokhtari, C. Oh, F. Pierce, and T. Rush, for their diligent efforts. We also thank the referees who have made extensive and very useful comments. Our work has been supported by NASA and the NSF.

7 References

1 J. C. Brinker and G. W. Scherer, *Sol Gel Science: The physics and chemistry of sol–gel processing*, 1990, Academic Press, New York.
2 D. Stauffer, *Introduction to Percolation Theory*, 1985, Taylor and Francis, London.
3 W. C. K. Poon and M. D. Haw, *Adv. Colloid Interface Sci.*, 1997, **73**, 71–126.
4 E. Zaccarelli, *J. Phys.: Condens. Matter*, 2007, **19**, 323101.
5 M. Kolb, R. Botet and R. Jullien, *Phys. Rev. Lett.*, 1983, **51**, 1123–1126.
6 T. Vicsek, *Fractal Growth Phenomena*, 1989, World Scientific, Singapore.
7 D. Fry, T. Sintes, A. Chakrabarti and C. M. Sorensen, *Phys. Rev. Lett.*, 2002, **89**, 148301–148304.
8 M. Rottereau, J. C. Gimel, T. Nicolai and D. Durand, *Eur. Phys. J. E*, 2004, **15**, 133–140.
9 M. Rottereau, J. C. Gimel, T. Nicolai and D. Durand, *Eur. Phys. J. E*, 2004, **15**, 141–148.
10 C. Oh and C. M. Sorensen, *J. Colloid Interface Sci.*, 1997, **193**, 17–25.
11 D. Fry, A. Chakrabarti, W. Kim and C. M. Sorensen, *Phys. Rev. E: Stat., Nonlinear, Soft Matter Phys.*, 2004, **69**, 061401–061410.
12 M. von Smoluchowski, *Phys. Z.*, 1916, **23**, 585.
13 S. K. Friedlander, *Smoke, Dust and Haze*, Oxford University Press, New York, 2000.
14 P. G. J. van Dongen and M. H. Ernst, *Phys. Rev. Lett.*, 1985, **54**, 1396–1399.
15 C. Oh and C. M. Sorensen, *J. Aerosol Sci.*, 1997, **28**, 937–957.
16 R. Jullien and R. Botet., *Aggregation and Fractal Aggregates*, 1987, World Scientific, Singapore.
17 C. M. Sorensen and G. Roberts, *J. Colloid Interface Sci.*, 1997, **186**, 447–452.
18 P. Meakin, *Phys. Rev. Lett.*, 1983, **51**, 1119–1122.
19 A. Hasmy and R. Jullien, *J. Non-Cryst. Solids*, 1995, **186**, 342–348.
20 J. C. Gimel, D. Durand and T. Nicolai, *Phys. Rev. B: Condens. Matter*, 1995, **51**, 11348–11357.
21 J. C. Gimel, T. Nicolai and D. Durand, *J. Sol-Gel Sci. Technol.*, 1999, **15**, 129–136.
22 M. C. Heine and S. E. Pratsinis, *Langmuir*, 2006, **22**, 10238–10245.
23 M. C. Heine and S. E. Pratsinis, *Langmuir*, 2007, **23**, 9882–9890.
24 S. Corezzi, C. De Michele, E. Zaccarelli, D. Fioretto and F. Sciortino, *Soft Matter*, 2008, **4**, 1173–1177.
25 S. Corezzi, C. De Michele, E. Zaccarelli, P. Tartaglia and F. Sciortino, *J. Phys. Chem. B*, 2009, **113**, 1233–1236.
26 F. Sciortino, C. De Michele, S. Corezzi, J. Russo, E. Zaccarelli and P. Tartaglia, *Soft Matter*, 2009, **5**, 2571–2575.
27 S. Corezzi, D. Fioretto, C. De Michele, E. Zaccarelli and F. Sciortino, *J. Phys. Chem. B*, 2010, **114**, 3769–3775.
28 R. M. Ziff, E. D. McGrady and P. Meakin, *J. Chem. Phys.*, 1985, **82**, 5269–5274.
29 M. Kolb, *Phys. Rev. Lett.*, 1984, **53**, 1653–1656.
30 M. Carpineti and M. Giglio, *Phys. Rev. Lett.*, 1992, **68**, 3327–3331.

31 R. Dhaubhadel, Ph.D. Thesis, Kansas State University, unpublished 2008.
32 C. M. Sorensen, W. B. Hageman, T. J. Rush, H. Huang and C. Oh, *Phys. Rev. Lett.*, 1998, **80**, 1782–1785.
33 H. Wu, J. Xie and M. Morbidelli, *Biomacromolecules*, 2005, **6**, 3189–3197.
34 R. Dhaubhadel, A. Chakrabarti and C. M. Sorensen, *Aerosol Sci. Technol.*, 2009, **43**, 1053–1063.
35 C. M. Sorensen, *Aerosol Sci. Technol.*, 2001, **35**, 648–687.
36 R. Dhaubhadel, G. Gerving, A. Chakrabarti and C. M. Sorensen, *Aerosol Sci. Technol.*, 2007, **41**, 804–810.
37 P. Meakin, *Adv. Colloid Interface Sci.*, 1987, **28**, 249–331.
38 M. Lattuada, H. Wu and M. Morbidelli, *J. Colloid Interface Sci.*, 2003, **268**, 106–120.
39 C. M. Sorensen and C. Oh, *Phys. Rev. E: Stat. Phys., Plasmas, Fluids, Relat. Interdiscip. Top.*, 1998, **58**, 7545–7548.
40 M. Lattuada, H. Wu, A. Hasmy and M. Morbidelli, *Langmuir*, 2003, **19**, 6312–6316.
41 A. Hasmy and R. Jullien, *Phys. Rev. E: Stat. Phys., Plasmas, Fluids, Relat. Interdiscip. Top.*, 1996, **53**, 1789–1794.
42 D. Fry, PhD Thesis, Unpublished, 2003, Kansas State University.
43 C. M. Sorensen, W. G. Kim, D. Fry and A. Chakrabarti, *Langmuir*, 2003, **19**, 7560–7563.
44 C. Oh and C. M. Sorensen, *J. Nanopart. Res.*, 1999, **1**, 369–377.
45 H. Huang, C. Oh and C. M. Sorensen, *Phys. Rev. E: Stat. Phys., Plasmas, Fluids, Relat. Interdiscip. Top.*, 1998, **57**, 875.
46 J. J. Cerda, T. Sintes, C. M. Sorensen and A. Chakrabarti, *Phys. Rev. E: Stat., Nonlinear, Soft Matter Phys.*, 2004, **70**, 051405.
47 G. Dietler, C. Aubert, D. S. Cannell and P. Wiltzius, *Phys. Rev. Lett.*, 1986, **57**, 3117–3120.
48 J. Bibette, T. G. Mason, H. Gang and D. A. Weitz, *Phys. Rev. Lett.*, 1992, **69**, 981–984.
49 W. G. Kim, C. M. Sorensen and A. Chakrabarti, *Langmuir*, 2004, **20**, 3969–3973.
50 W. G. Kim, C. M. Sorensen, D. Fry and A. Chakrabarti, *J. Aerosol Sci.*, 2006, **37**, 386–401.
51 C. M. Sorensen and W. B. Hageman, *Langmuir*, 2001, **17**, 5431–5434.
52 R. Dhaubhadel, F. Pierce, A. Chakrabarti and C. M. Sorensen, *Phys. Rev. E: Stat., Nonlinear, Soft Matter Phys.*, 2006, **73**, 011404.
53 H. Wu, J. Xie, M. Lattuada and M. Morbidelli, *Langmuir*, 2005, **21**, 3291–3295.
54 P. Wong and Q. Cao, *Phys. Rev. B: Condens. Matter*, 1992, **45**, 7627–7632.
55 T. Mokhtari, A. Chakrabarti, C. M. Sorensen, C.-Y. Cheng and D. Vigil, *J. Colloid Interface Sci.*, 2008, **327**, 216–223.

